Available online at www.sciencedirect.com
SCIENCE DIRECT®
Journal of Sound and Vibration 262 (2003) 309–331
JOURNAL OF SOUND AND VIBRATION
www.elsevier.com/locate/jsvi

The experimental validation of a numerical model for the prediction of the vibrations in the free field produced by road traffic

G. Lombaert, G. Degrande*

Department of Civil Engineering, K.U. Leuven, Kasteelpark Arenberg 40, B-3001 Leuven, Belgium

Received 13 September 2001; accepted 14 February 2002

Abstract

The objective of the present paper is the experimental validation of a numerical model for the prediction of traffic-induced vibrations. The vibrations in the free field, generated by the passage of a vehicle on an uneven road, are predicted in two stages. First, the equations of motion of the vehicle are solved to determine the dynamic axle loads. Next, these axle loads are applied to the road and the free field vibrations are computed. An elaborate measurement campaign has been set up to validate this model. The response of a Volvo FL6 truck and the response in the free field have been measured simultaneously during the passage of the truck over an artificial road unevenness. The parameters related to the vehicle, the road and the soil have been determined experimentally. A comparison of the predicted and the measured response demonstrates the predictive qualities of the numerical model. Furthermore, the results provide a clear insight in the influence of the vehicle speed on the vehicle's and the free field response.

1. Introduction

The study of traffic-induced vibrations is a three-dimensional, dynamic soil–structure interaction problem, where wave propagation in the soil couples the source and the receiver. Three sub-problems can be distinguished: the characterization of the source, wave propagation in the soil and the interaction of the incident wave field and the structure. Due to the intricacy of the coupled problem, prediction models often only consider the vibrations in the free field.

The dynamic vehicle–road interaction is theoretically a coupled problem that requires a simultaneous solution of the equations of motion of the vehicle and the road. Due to the large

*Corresponding author. Tel.: +32-16-32-16-67; fax: +32-16-32-19-88.
E-mail address: geert.degrande@bwk.kuleuven.ac.be (G. Degrande).

0022-460X/03/$ - see front matter
PII: S0022-460X(02)01048-9

stiffness of the road compared to the vehicle's tyre or suspension stiffness, the problem can be uncoupled, as indicated by Cebon [1] and Gillespie et al. [2]. This enables the prediction of the free field vibrations in two stages. First, the road is assumed to be infinitely rigid and the vehicle's response is computed. Next, the dynamic axle loads are applied to the road and the response in the free field is determined.

Courage [3], Hao and Ang [4], Hunt [5] and the CUR in the Netherlands [6] have proposed similar numerical models for the prediction of free field traffic-induced vibrations. The global road unevenness is described in a stochastic way by a power spectral density function (PSD) [7,8]. A linear vehicle model is used to compute the PSD of the dynamic axle loads by means of frequency response functions (FRF). Furthermore, a continuous stream of vehicles is considered, for which it is assumed that the response for a receiver at a large distance with respect to the mean vehicle spacing is stationary. As a result, the motion of the vehicle can be neglected and stationary stochastic methods are applied to compute the PSD of the free field vibrations from the PSD of the axle loads.

Al-Hunaidi [9] and Watts [10] observe that practical vibration problems are related to discrete irregularities, such as potholes and joints in a concrete road surface. Watts and Krylov [11] have studied ground-borne vibrations due to vehicles crossing road humps and speed control cushions. The peak particle velocity of the soil at 6 m from the nearside wheel track during the passage of 11 types of vehicles on eight types of test profiles and at four vehicle speeds (15, 25, 35 and 45 km/h) has been measured. The response has been compared with numerical predictions, based on a one-axle vehicle model and the Green's functions of a half-space. An empirical relation has been derived to extrapolate the test results to sites with different soil conditions, enabling the determination of minimum distances of speed control cushions and road humps from building foundations on different types of soil. Although this study presents very valuable data, its major drawback is that a simplified numerical prediction model is used, where the layering of the soil is not accounted for, while material and radiation damping are represented by a single exponent in the empirical relations.

In the present paper, an advanced numerical model accounting for dynamic road–soil interaction as well as the layered structure of the soil [12] will be validated. Road unevenness is described by a deterministic function. Local as well as global road unevenness can be described in this way. The free field vibrations are predicted in two stages, uncoupling the prediction of the vehicle's response from the road–soil interaction problem. A substructure method is applied to solve the road–soil interaction problem [13].

In order to validate this model, an initial measurement programme was performed at the test circuit of the truck manufacturer DAF in Sint-Oedenrode (The Netherlands). The response of a DAF FT 85 truck with trailer and the response in the free field have been measured during 10 passages of the truck on an artificial uneven surface. These measurements have been used for a preliminary validation of the numerical model [14]. A thorough validation, however, requires measurements where more attention goes to the experimental determination of the parameters related to the vehicle, the road and the soil.

More elaborate experiments were performed in June 2000 at the 'de Hemptinne site' of the Belgian Army in Heverlee (Belgium) [15]. The truck's response and the free field response were measured during 26 passages of a Volvo FL6 truck on the artificial road unevenness at vehicle speeds between 23 and 58 km/h. Compared to the first measurement campaign, the free field

response was measured at a larger number of points, more vehicle passages have been recorded and more attention went to the experimental determination of the model parameters.

The objective of this paper is to use these results for the validation of the numerical prediction model for traffic-induced vibrations. The model is only briefly discussed and the reader is referred to other publications for a detailed mathematical description [16,12]. Attention is paid to the various parameters related to the vehicle, the road and the soil. Finally, the predicted and the measured response are compared to check the predictive qualities of the numerical model.

2. Numerical model

The uncoupling of the calculation of the vehicle's and the free field response enables a prediction of the free field response in two stages. First, the equations of motion of the vehicle are solved and the dynamic axle loads are computed. Next, these axle loads are applied to the road and the road–soil interaction problem is solved.

The dynamic component of the axle loads is induced by the road unevenness and depends on the road profile, the vehicle characteristics and the vehicle speed. The basic mathematical models for the simulation of vehicle ride behaviour are also used to predict the dynamic axle loads. These vehicle models are composed of discrete masses, springs, friction elements and dampers (Fig. 1). A linear 2-D vehicle model with a limited number of degrees of freedom (DOF) is used to calculate the dynamic axle loads from the longitudinal road unevenness.

In the case where a linear vehicle model is used, the dynamic axle loads can be computed by FRF [1,17,12]. The FRF $\hat{h}_{f_k u_l}(\omega)$ represents the frequency content of the kth axle load due to a harmonic excitation at the contact point of axle l with the road. Accounting for the time delay between the input at the different vehicle axles, the contribution of all axles l can be collected into a single FRF $\hat{h}_{f_k u}(\omega)$.

Two groups of eigenmodes dominate the response of the vehicle in the vertical plane: the pitch and bounce modes at relatively low eigenfrequencies between 0.8 and 3 Hz and the axle hop modes at frequencies between 8 and 15 Hz. The axle hop modes play a crucial role in the generation of traffic-induced vibrations [18,19].

A forward Fourier transformation of the longitudinal road unevenness $u_{w/r}(y)$ to the wavenumber domain reveals the content $\tilde{u}_{w/r}(k_y)$ of the profile in terms of the wavenumber k_y

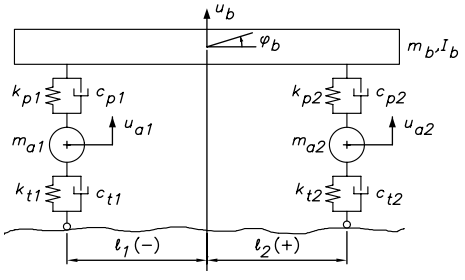

Fig. 1. 2-D 4DOF model for a passenger car or a truck with two axles.

or the wavelength $\lambda_y = 2\pi/k_y$. For regular vehicle speeds between 8 and 20 m/s, the range of wavenumbers k_y that leads to an excitation of the vehicle at the axle hop frequencies is situated between 2.5 and 12 rad/m or wavelengths λ_y between 0.5 and 2.5 m [16].

The dynamic road–soil interaction problem is first solved for an implusive load that is applied at a fixed position (Fig. 2). Following the solution procedure presented by Clouteau [20] and Aubry et al. [13], the equations of motion of the coupled road–soil system are derived in the frequency-wavenumber domain (x, k_y, z, ω), where the co-ordinate y along the road is transformed to the wavenumber k_y by means of a forward Fourier transformation [13,12]. The road is modelled as an elastic beam with a rigid cross-section at the surface of an elastic horizontally layered half-space. Both the road's bending and torsional deformations are accounted for. The computation of the soil's impedance requires the calculation of the soil tractions at the road–soil interface for the bending and torsional modes. A boundary element method (BEM) is applied to calculate the soil tractions [13,12]. The BEM is based on the Green's functions of the layered half-space, which are calculated by means of the direct stiffness method [21,22].

The solution of the road–soil interaction problem results in the modal co-ordinates $\tilde{\boldsymbol{\alpha}}$ of the bending and torsional modes of the road in the frequency-wavenumber domain. This solution allows the tractions at the road–soil interface to be determined. The dynamic reciprocity theorem is used to calculate the response in the free field for a fixed implusive load from the soil tractions and the Green's functions of the layered half-space. The free field response serves as a transfer function, denoted as $\tilde{h}_{zi}(\xi_1, k_y, \xi_3, \omega)$ for the displacement component in the direction $\mathbf{e}_i$.

Finally, the dynamic Betti–Rayleigh reciprocal theorem is used to compute the free field response for the moving axle loads. The motion of the source position is replaced by an equivalent motion of the receiver position. The transfer function derived previously for a fixed impulsive load on the road is now employed for the calculation of the free field response. In the frequency-wavenumber domain, the response $\tilde{u}_{si}(\xi_1, k_y, \xi_3, \omega)$ is calculated as the product of the transfer function $\tilde{h}_{zi}(\xi_1, k_y, \xi_3, \omega)$ and the load $\hat{g}_k(\omega - k_y v)$, shifted by $k_y v$. This shift represents phenomena as the Doppler effect. A double inverse Fourier transformation from k_y to y and from ω to t yields the time history $u_{si}(\xi_1, \xi_2, \xi_3, t)$ of the response.

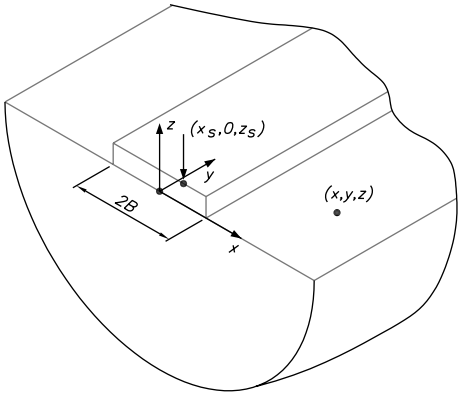

Fig. 2. The road–soil interaction problem.

3. The experimental configuration

3.1. The artificial unevenness

The artificial unevenness has the shape of a traffic plateau with straight ramps and is composed of two three-ply boards (Fig. 3). The design of the artificial unevenness is based on the frequency content of the signal that is applied to the vehicle's axles. Each board is composed of three plates and has a total height H of 0.054 m, a flat top part with a length $L = 1.30$ m and a width of 1 m. The upper two plates have sloping ends, resulting in slopes with a length $l = 0.20$ m.

For the calculation of the vehicle's response, the bottom plate of the profile is assumed to have sloping ends as well. The length l of the slopes equals 0.30 m, the base length equals $L + 2l = 1.90$ m and the mean length is equal to $L + l = 1.60$ m. Fig. 4a shows the longitudinal unevenness profile $u_{w/r}(y)$ as a function of the co-ordinate y along the road.

The wavenumber content (Fig. 4b) is mainly situated at wavenumbers k_y below 20 rad/m or wavelengths $\lambda_y = 2\pi/k_y$ larger than 0.30 m. The separation between the lobes is inversely proportional to the mean length $L + l$ of the profile. The zero values correspond to $k_{yn}^0 = 2\pi n/(L + l)$, while local maxima occur at approximately $k_{yn}^{max} = 3\pi n/(L + l)$.

The frequency content $\hat{u}_{w/r}(\omega)$ of the signal that is applied to the vehicle's axles is calculated from the representation in the wavenumber domain as $\tilde{u}_{w/r}(-\omega/v)/v$ [12]. For a fixed vehicle speed v, the frequency content is zero at frequencies $f_n^0 = nv/(L + l)$, while local maximum occur at $f_n^{max} = 3nv/2(L + l)$. Fig. 5 illustrates that, for increasing vehicle speeds, the quasi-static value of the signal decreases and the frequency content shifts to higher frequencies. In the frequency range where the axle hop frequencies are situated, there is a large variation of the signal, which will subsequently affect the frequency content of the axle loads.

The artificial unevenness has been installed on a road with a smooth asphalt surface at the 'de Hemptinne' site (Fig. 3) of the Belgian Army in Heverlee. At this site, the response of a Volvo FL6 truck and the response in the free field are measured during 26 passages of the truck on the artificial unevenness. The vehicle speed is varied with steps of 5 km/h from 25 km/h upto

Fig. 3. The profile installed at the test site.

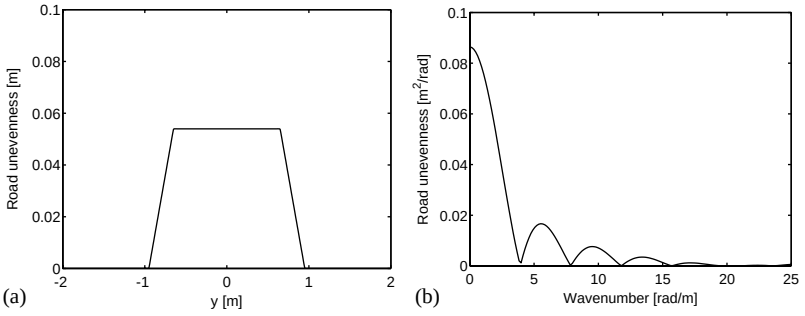

Fig. 4. The longitudinal profile of the artificial unevenness (a) as a function of the co-ordinate y along the road and (b) in the wavenumber domain. (a) $u_{w/r}(y)$; (b) $\tilde{u}_{w/r}(k_y)$.

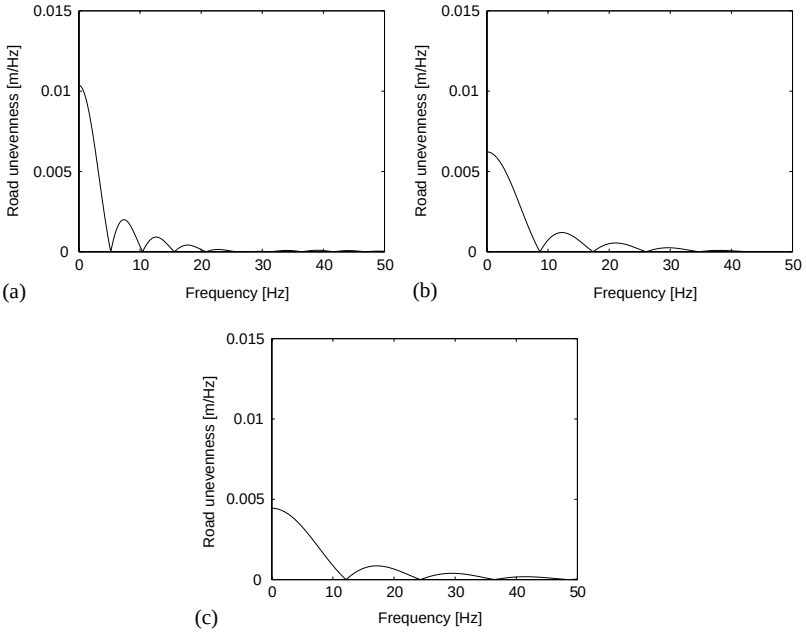

Fig. 5. The unevenness experienced by the vehicle at a speed (a) $v = 30$ km/h, (b) $v = 50$ km/h and (c) $v = 70$ km/h.

60 km/h, with an average of three passages per vehicle speed. During the experiments, a GATSO 24 radar has been used for the measurement of the vehicle speed.

3.2. The vehicle

The Volvo FL6 truck is a two-axle truck with a wheel base $w = 5.20$ m (Fig. 3). It has a steel leaf suspension at the front and the rear axle. A peak-picking method and a stochastic subspace identification (SSI) method [23] are applied to estimate the pitch and bounce and the axle hop frequencies from the measured truck response [15].

A 2-D 4DOF vehicle model (Fig. 1) is used to predict the vehicle's response and the dynamic axle loads. The parameters of the model are determined by means of truck weighings, data provided by the truck manufacturer and a fit of the measured and predicted vehicle response [15].

The mass m_b of the vehicle body and the front and rear axle mass m_{a1} and m_{a2} have been determined from the weighings and the information of the truck manufacturer. The rotational inertia I_b and the range of values reported by the manufacturer for the spring constants k_{p1} and k_{p2} of the suspension system and the spring constants k_{t1} and k_{t2} of the tyres have been used to tune the eigenfrequencies of the model. The damping coefficients c_{t1} and c_{t2} of the rear and the front tyre are assumed to be zero. The damping coefficients c_{p1} and c_{p2} of the front and rear suspension system are estimated through a fit of the predicted and measured frequency content of the response at the axle hop frequencies for a vehicle speed $v = 30$ km/h.

The following values are found: $m_b = 9000$ kg, $I_b = 35\,000$ kgm^2, $m_{a1} = 600$ kg, $m_{a2} = 400$ kg, $l_1 = -1.49$ m, $l_2 = 3.72$ m, $k_{p1} = 0.61 \times 10^6$ N/m, $k_{p2} = 0.32 \times 10^6$ N/m, $k_{t1} = 3.00 \times 10^6$ N/m, $k_{t2} = 1.50 \times 10^6$ N/m, $c_{p1} = 16\,000$ N s/m, $c_{p2} = 10\,050$ N s/m, $c_{t1} = 0$ N s/m and $c_{t2} = 0$ N s/m.

Fig. 6 shows the modulus of the FRF $\hat{h}_{f_k u_l}(\omega)$ of the vehicle model. The FRF $\hat{h}_{f_k u_k}(\omega)$ represent the frequency content of the axle load at axle k for an impulse excitation at the same axle and exhibit a peak value at the axle hop frequency. The FRF $\hat{h}_{f_k u_k}(\omega)$ have a larger amplitude than the FRF $\hat{h}_{f_k u_l}(\omega)$ for an excitation at a different axle l. The latter have a peak at the pitch and bounce mode.

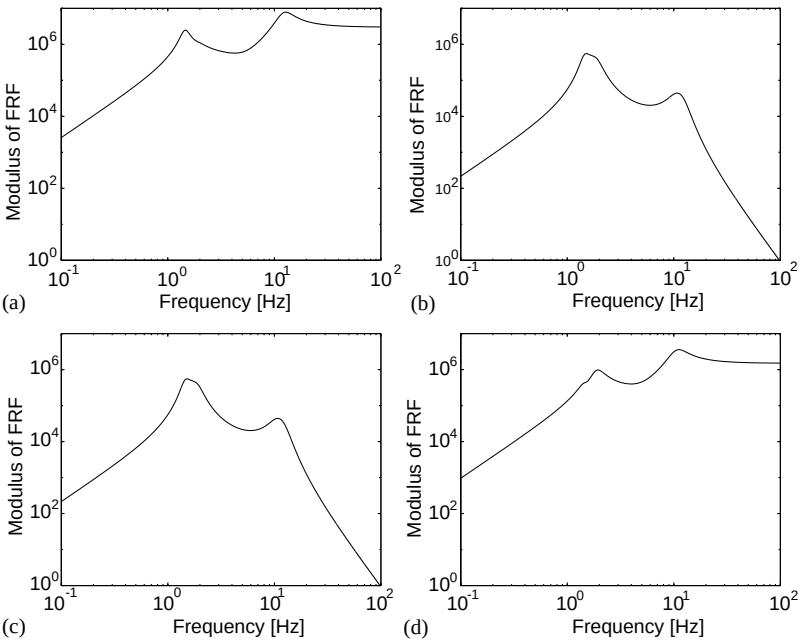

Fig. 6. Modulus of the FRF $\hat{h}_{f_k u_l}(\omega)$ for the 2-D 4DOF vehicle model of the Volvo FL6 truck. (a) $\hat{h}_{f_1 u_1}(\omega)$, (b) $\hat{h}_{f_1 u_2}(\omega)$, (c) $\hat{h}_{f_2 u_1}(\omega)$ and (d) $\hat{h}_{f_2 u_2}(\omega)$.

3.3. The road

The road has a total width $2B = 6.20$ m and is composed of an asphalt top layer and a foundation that is composed of a crushed stone layer and a crushed concrete layer.

A spectral analysis of surface waves (SASW) test has been performed to determine the road's stratification and the dynamic road characteristics [24]. An inversion procedure with the profile of a single layer on a half-space reveals the presence of the asphalt top layer with a thickness of 0.15 m and a shear wave velocity $C_s = 1600$ m/s on top of a half-space with a shear wave velocity $C_s = 250$ m/s [24]. An inversion procedure with more layers on top of a half-space does not result in a refinement of this profile. The characteristics of the half-space are therefore also influenced by the presence of the road's foundation under the asphalt top layer.

For an estimated asphalt density $\rho = 2100$ kg/m^3 and a Poisson ratio $\nu = 1/3$, the Young's modulus E equals $14\,340 \times 10^6$ N/m^2. The Young's modulus of asphalt is very sensitive to the temperature, however. During the experiments in June, the temperature was about 20°C, while during the SASW test in December, the temperature was 5°C. The approximating relation $E = 10^{(a+bT)}$ [25], with $b = -0.013$, results in an estimated value for E of 9150×10^6 N/m^2 at a temperature of 20°C. This corresponds well with values that are reported in literature for the Young's modulus of asphalt during spring and summer [26].

Table 1 summarizes the layer thickness d, the Poisson ratio ν, the density ρ and Young's modulus E as used for the road model. The thickness of the crushed stone layer and the crushed concrete layer correspond to design values. The dynamic characteristics of these layers are estimated [26] and assumed to be insensitive to the temperature.

In the numerical model, the road is modelled as a beam with a width $2B = 6.20$ m and a rigid cross-section, characterized by a bending stiffness EI, a mass per unit length ρA, a torsional stiffness GC and a torsional moment of inertia ρI_p. The material properties E, ν, ρ and the thickness d of each layer in Table 1 are used to calculate these equivalent properties as $EI = 7.83 \times 10^7$ N m^2, $\rho A = 7099$ kg/m, $GC = 1.08 \times 10^8$ N m^2 and $\rho I_p = 2.32 \times 10^4$ kg m.

3.4. The soil

The soil at the 'de Hemptinne' test site is mainly composed of loam. Both a SASW test [27] and a seismic cone penetration test (SCPT) [24] have been performed to determine the soil's stratification and the dynamic soil characteristics. The results of the SASW test reveal the dynamic

Table 1
The parameters of the road model

Layer type	d (m)	ν (−)	ρ (kg/m^3)	E ($\times 10^6$ N/m^2)
1 Asphalt	0.15	0.33	2100	9150
2 Crushed stone	0.19	0.50	2000	500
3 Crushed concrete	0.25	0.50	1800	200

characteristics of the upper soil layers. The SCPT has been performed at a distance of 12 and 36 m from the road's axis. At both locations, a stiff layer at a depth of 8.20 m could not be penetrated.

Fig. 7a shows, on the same graph, the shear wave velocity profile as obtained with the SASW test and the SCPT. At intermediate depths, the results correspond well. The results of the SASW test are more detailed at the soil's surface, while the results of the SCPT indicate the presence of a stiff layer at a depth of 8.20 m. The higher shear wave velocities at smaller depths are probably due to wave refractions. Fig. 7b shows the longitudinal wave velocity profile as obtained with the SCPT. The relation between the shear wave velocity and the longitudinal wave velocity allows to estimate the Poisson ratio ν. For the top layers, a Poisson ratio of 1/3 is found, while at a depth larger than 2.3 m, the Poisson ratio is equal to 0.47. This high value reveals the presence of the ground water table.

Based on these observations, the soil's density ρ is estimated as 1900 kg/m^3 for the dry loam layers up to a depth of 2.3 m and 2000 kg/m^3 for the saturated loam layers at larger depths. The results of the SASW test for the shear wave velocity C_s and the layer thickness d have been combined with the results for the Poisson ratio ν to determine the modulus of Young E of the upper four soil layers of the soil model (Table 2). The shear wave velocity profile of the soil model therefore coincides with the shear wave velocity profile as obtained with the SASW test for the

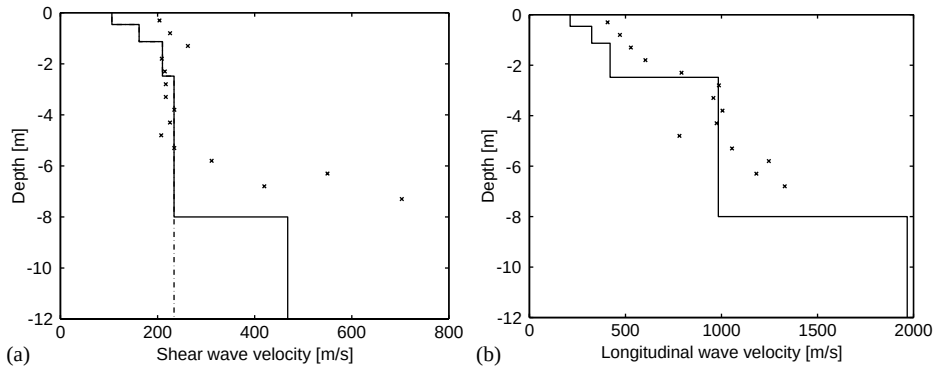

Fig. 7. (a) The shear wave velocity profile as obtained with the SASW test (dash–dotted line) and the SCPT (crosses), and the profile as used in the soil model (solid line). The latter coincides with the profile from the SASW test up to a depth of 8.20 m. (b) The longitudinal wave velocity profile as obtained with the SCPT (crosses), and the profile as used in the soil model (solid line). (a) Shear wave velocity and (b) longitudinal wave velocity.

Table 2
The parameters of the soil model

Layer	d (m)	ν (−)	ρ (kg/m^3)	E ($\times 10^6$ N/m^2)	C_s (m/s)	C_p (m/s)	β (−)
1	0.46	0.33	1900	57	106	212	0.0500
2	0.67	0.33	1900	133	162	324	0.0375
3	1.35	0.33	1900	223	210	420	0.0250
4	5.72	0.47	2000	322	234	984	0.0250
5	∞	0.47	2000	1288	468	1968	0.0250

upper four soil layers of the model (Fig. 7a). At a depth of 8.20 m, a layer with a stiffness that is arbitrarily taken as four times the stiffness of the fourth layer is introduced (Figs. 7a and 7b).

Table 2 summarizes the layer thickness d, the Poisson ratio ν, the density ρ and Young's modulus E used for the soil model. The hysteretic material damping ratio β has a large influence on the response at distances from the source that are large with respect to the dominant wavelength in the soil. However, it has not been included in the inversion process for the determination of the soil characteristics from the SASW data. The material damping is estimated to be 0.050 for the first layer, 0.0375 for the second layer and 0.025 for the deeper layers. This agrees with the experimental observation that material damping decreases with depth.

The total thickness of the road roughly corresponds to the thickness of the top layer of the soil model (Table 2). As in the numerical model the road is assumed to be located at the soil's surface, the influence of the top layer is discarded for the solution of the dynamic road–soil interaction problem. A soil model is considered that consists of the layers 2 to 4 of the soil profile in Table 2, supported by the half-space. This soil model is referred to as soil model 1. The BEM for the calculation of the soil's impedance is based on the Green's functions that represent the fundamental response of the soil model 1 for a vertical impulse load at the surface of the half-space (Fig. 8a). The solution of the road–soil interaction problem yields the soil tractions at the interface between the road and the soil.

For the calculation of the response in the free field or the transfer function between the road and the soil, a second soil model is used that consists of layers 1–4, supported by the half-space (Table 2). This soil model is referred to as soil model 2. In this case, the Green's functions are calculated for the case where a vertical impulse load is applied at the interface between the layers 1 and 2 (Fig. 8b).

4. The validation of the vehicle's response

4.1. The predicted axle loads

Figs. 9 and 10 illustrate the prediction of the front axle load at a vehicle speed v equal to 30 and 58 km/h, respectively. A time scale is chosen where the time $t = 0$ corresponds to the time at which the front axle of the vehicle is located at the middle of the profile.

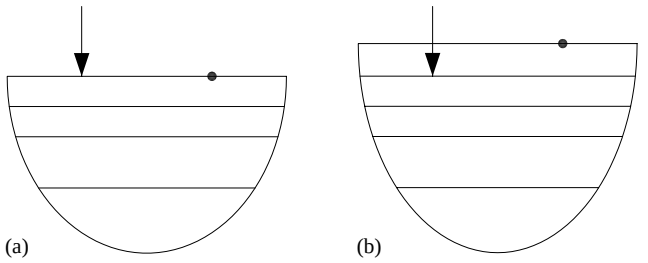

Fig. 8. The source–receiver configuration for the calculation of the Green's functions used for the computation of (a) the soil's impedance and (b) the road–soil transfer functions. (a) Soil model 1 and (b) soil model 2.

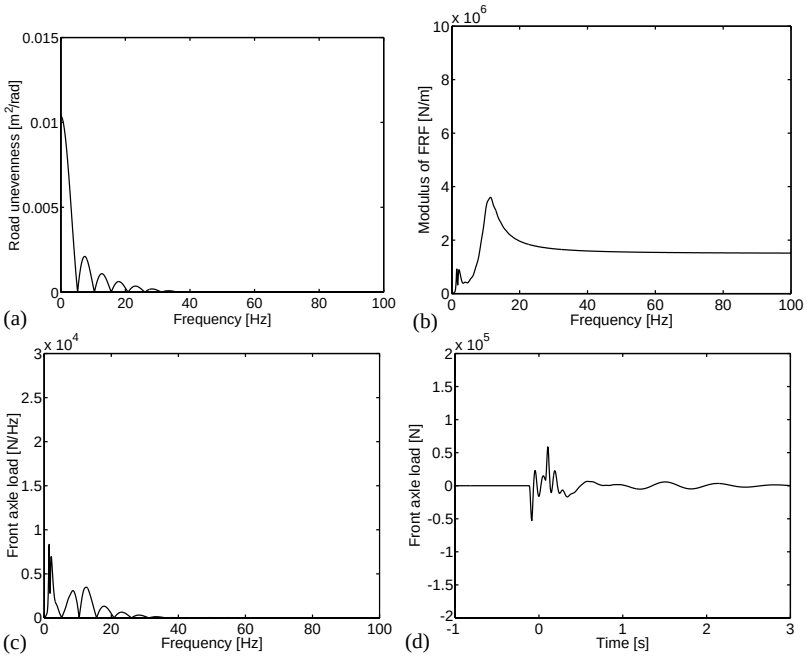

Fig. 9. (a) Frequency content $\hat{u}_{w/r}(\omega)$ of the experienced unevenness, (b) FRF $\hat{h}_{f_2u}(\omega)$, (c) frequency content $\hat{g}_2(\omega)$ and (d) time history $g_2(t)$ of the predicted front axle load for the passage of the Volvo FL6 truck on the artificial profile at a vehicle speed $v = 30$ km/h. (a) $\hat{u}_{w/r}(\omega)$, (b) $\hat{h}_{f_2u}(\omega)$, (c) $\hat{g}_2(\omega)$ and (d) $g_2(t)$.

Figs. 9a and 10a show the frequency content $\hat{u}_{w/r}(\omega)$ of the unevenness as it is experienced by the front axle. As has been shown in Fig. 5, the frequency content shifts to higher frequencies while the quasi-static value decreases for an increasing vehicle speed v. Figs. 9b and 10b represent the FRF $\hat{h}_{f_2u}(\omega)$ for the front axle load. Figs. 9c and 10c show the frequency content $\hat{g}_2(\omega)$ of the front axle load, which is obtained as the product of the frequency content $\hat{u}_{w/r}(\omega)$ of the unevenness and the FRF $\hat{h}_{f_2u}(\omega)$. Whilst the frequency content of the axle load is mainly situated below 30 Hz for a vehicle speed v of 30 km/h, this upper limit shifts to 60 Hz for $v = 58$ km/h. The dominant frequency, however, remains approximately constant and is mainly determined by the axle hop frequency of the front axle. The contribution at the pitch and bounce frequencies is relatively small.

Figs. 9d and 10d finally show the time history $g_2(t)$ of the front axle load, which is obtained through an inverse FFT. The duration of the signal can be estimated from the mean length $L + l = 1.60$ m of the profile, the wheel base $w = 5.20$ m of the truck and the vehicle speed v. At a speed $v = 30$ km/h, a transient signal with a duration of 0.82 s is expected. At a time $t = -0.10$ s, the front axle ascends the profile, while at $t = 0.10$ s, the front axle descends. At $t = 0.53$ and 0.72 s, the ascending and descending of the rear axle can hardly be observed, which illustrates that the interaction between the axles is small.

At a speed $v = 58$ km/h, the time delay between the ascending and the descending is reduced to 0.10 s. The peak axle load increases slightly for higher vehicle speeds.

Analogous conclusions can be drawn from the results for the rear axle load.

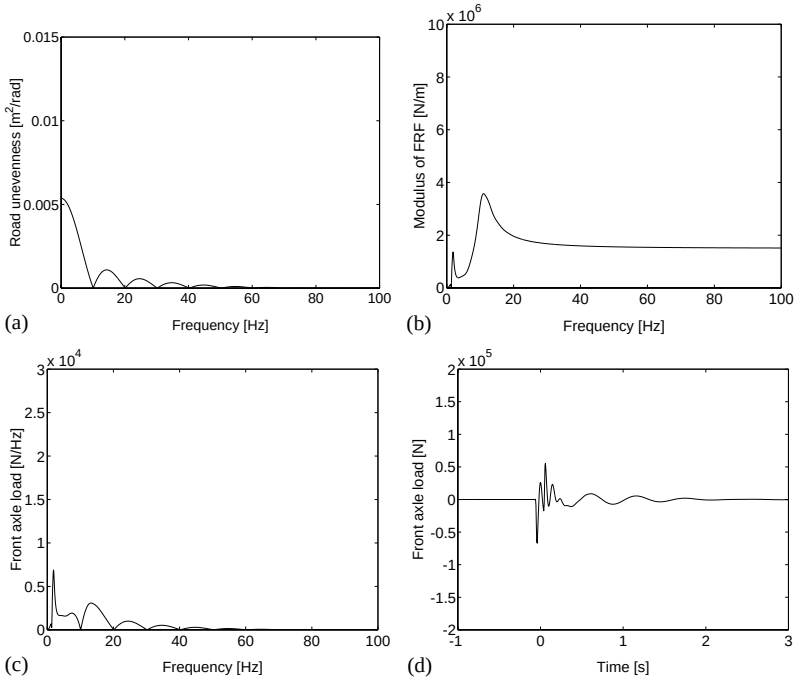

Fig. 10. (a) Frequency content $\hat{u}_{w/r}(\omega)$ of the experienced unevenness, (b) FRF $\hat{h}_{f_2u}(\omega)$, (c) frequency content $\hat{g}_2(\omega)$ and (d) time history $g_2(t)$ of the predicted front axle load for the passage of the Volvo FL6 truck on the artificial profile at a vehicle speed $v = 58$ km/h. (a) $\hat{u}_{w/r}(\omega)$, (b) $\hat{h}_{f_2u}(\omega)$, (c) $\hat{g}_2(\omega)$ and (d) $g_2(t)$.

4.2. Time history and frequency content of the axles' response

The truck's axle accelerations have been measured at the right-hand side of the vehicle. The experimental configuration consists of 2 PCB accelerometers with a sensitivity of 0.1 V/g, a portable PC and an OROS OR25 PcPackII Model 304 system, used for the power supply, anti-aliasing filter and A/D conversion at a sampling rate $f_s = 512$ Hz.

The accelerations of the axles are referred to by a label `TIAz`, where the character I indicates the location of the accelerometer at the front (F) or the rear (R) part of the truck. The characters A and z indicate that the vertical acceleration of the axle is considered.

Fig. 11 shows the time history and the frequency content of the predicted and the measured accelerations of the front axle for vehicle speeds of 30 and 58 km/h. Compared to Figs. 9 and 10, a time shift has been applied to the predicted results to synchronize both signals.

The time between the ascending and descending of one axle on the profile decreases from 0.19 s for a vehicle speed v of 30 km/h to 0.10 s for $v = 58$ km/h. The separate impacts at the ascending and descending of the axle can only be observed at the lowest vehicle speed.The duration of the transient signal is well predicted, whereas the peak acceleration is underestimated. The underestimation increases with the vehicle speed v. The frequency content of both the predicted and the measured acceleration is dominated by the axle hop frequencies and shifts to higher frequencies for an increasing vehicle speed. As the parameters of the 2-D vehicle model have been tuned using the vehicle's response at a speed of 30 km/h, it is not surprising that the axle's

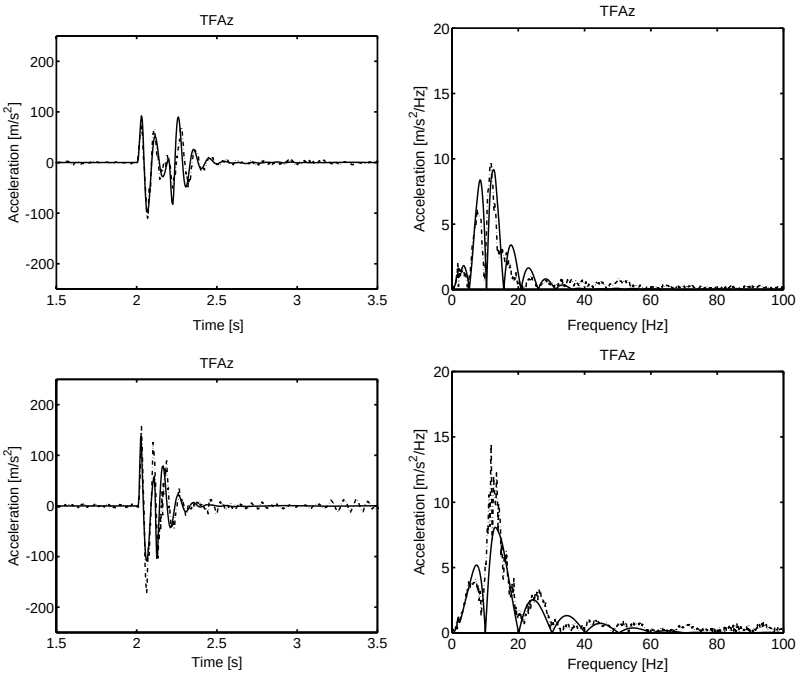

Fig. 11. Predicted (solid line) and measured (dash–dotted line) time history (left-hand side) and frequency content (right-hand side) of the acceleration of the front axle for vehicle speeds $v = 30$ km/h (top) and $v = 58$ km/h (bottom).

response at this vehicle speed is very well predicted. At higher vehicle speeds, the contribution at the axle hop frequency is underestimated.

Fig. 12 shows the time history and the frequency content of the predicted and the measured accelerations of the rear axle for vehicle speeds of 30 and 58 km/h. The quality of the prediction is less accurate than for the front axle. Although the peak accelerations correspond well, there is a clear difference between the duration of the predicted and the measured transient acceleration signal. This confirms the experimental observation of a loss of contact between the rear axle and the artificial profile, that is followed by an impact when the axle touches the road [15]. This phenomenon is not taken into account with the present linear vehicle model. As a result, the lobes that correspond to the frequency content of the unevenness signal are not present in the frequency content of the measured axle load. At higher vehicle speeds, this results in an important difference between the predicted and the measured axle load at a frequency of approximately 10 Hz. Furthermore, the contribution at low and high frequencies is underestimated.

4.3. *Peak acceleration of the axles' response*

Fig. 13a shows the measured and predicted peak acceleration of the truck's front axle as a function of the vehicle speed. At low vehicle speeds, the correspondence between the predicted and the measured peak acceleration is relatively good. At higher vehicle speeds, the peak acceleration of the front axle is underestimated.

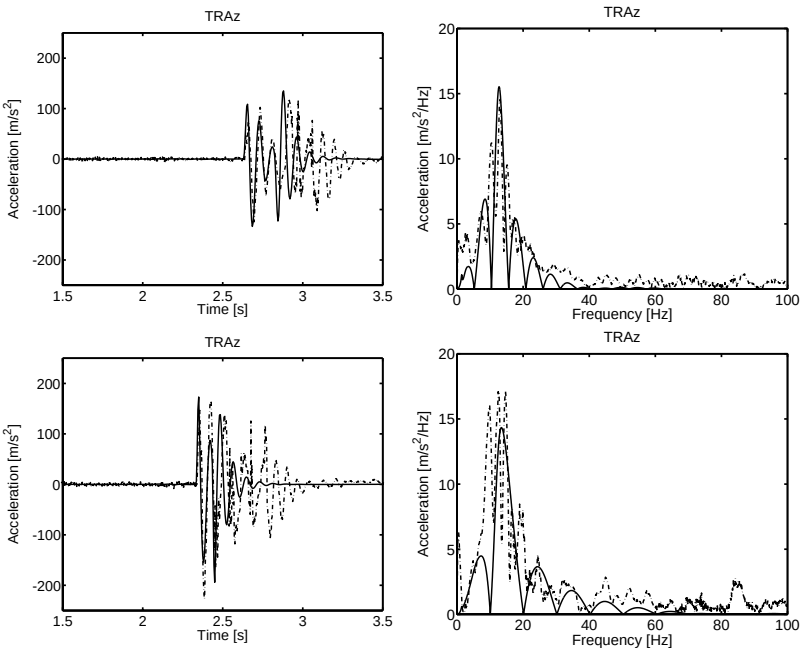

Fig. 12. Predicted (solid line) and measured (dash–dotted line) time history (left-hand side) and frequency content (right-hand side) of the acceleration of the rear axle for vehicle speeds $v = 30$ km/h (top) and $v = 58$ km/h (bottom).

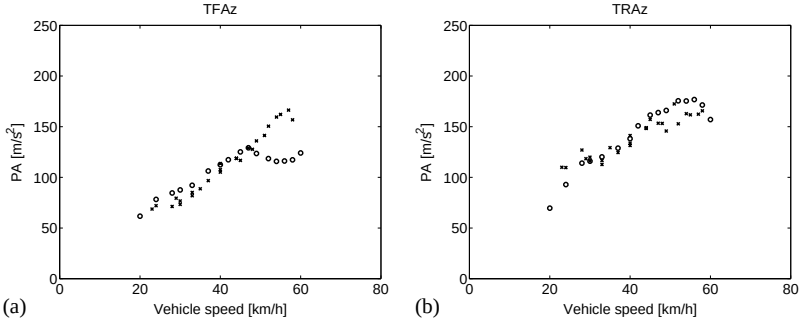

Fig. 13. Predicted (circles) and measured (crosses) peak axle acceleration of (a) the front axle and (b) the rear axle as a function of the vehicle speed. (a) Front axle and (b) rear axle.

For an increasing vehicle speed v, the frequencies $f_n^0 = nv/(L + l)$ and $f_n^{max} = 3nv/2(L + l)$, that characterize the zeros and the local maxima of the unevenness signal (Figs. 9a and 10a), shift to higher frequencies. As a result, the location of these frequencies changes with respect to the axle hop frequency of the front axle at 10.8 Hz. For a vehicle speed $v = 31.1$ km/h, the second zero f_2^0 is equal to the axle hop frequency. As the vehicle speed increases to 41.5 km/h, the first local maximum f_1^{max} of the experienced unevenness approaches the axle hop frequency and the peak acceleration increases. For a vehicle speed between 41.5 and 62.2 km/h, the axle hop frequency is situated between f_1^{max} and f_1^0 and the peak acceleration does not increase with the vehicle speed.

The peak acceleration is, however, not only determined by the amplitude of the frequency content of the axle's acceleration at the axle hop frequency and the observed trend in Fig. 13a is more complex. It illustrates, nevertheless, how the influence of the vehicle speed depends on the dynamic characteristics of the vehicle and the longitudinal unevenness profile.

Fig. 13b shows the measured and predicted peak acceleration of the truck's rear axle as a function of the vehicle speed. Although the loss of contact is not predicted, there is good agreement between the predicted and the measured peak acceleration of the rear axle. For a vehicle speed of 35.7 km/h, the frequency f_2^0 coincides with the axle hop frequency of the rear axle at 12.4 Hz. As the vehicle speed increases to 47 km/h, f_1^{max} tends to the axle hop frequency and the peak acceleration increases. For a vehicle speed between 47 and 71 km/h, the axle hop frequency is situated between f_1^{max} and f_1^0 and the peak acceleration is not expected to increase with the vehicle speed. This trend, however, cannot be detected in the variation of the measured peak acceleration with the vehicle speed. This is due to the loss of contact between the rear axle and the road. As a result, the frequency content of the rear axle acceleration (Fig. 12) does not show the lobes that characterize the unevenness (Fig. 11a).

5. The validation of the soil's response

5.1. Time history and frequency content of the free field response

The experimental configuration consists of 14 PCB seismic accelerometers, a KEMO VBF 35 unit and a 16 bit Daqbook 216 data-acquisition system, coupled to a portable PC. The A/D conversion is performed at a sampling rate $f_s = 500$ Hz. The vertical acceleration is measured at points, located at a distance between 4 and 48 m from the centre of the road (Fig. 14). At 8, 16 and at 24 m, the horizontal accelerations in both directions are also measured. Each accelerometer is mounted on a separate aluminium stake with a cruciform cross-section.

The free field velocities are calculated from the predicted axle loads (Figs. 9 and 10) and the transfer functions between the road and the soil by means of the Betti–Rayleigh reciprocal theorem. Fig. 15 shows the predicted and measured time history of the components v_x, v_y and v_z of the velocity at 8, 16 and 24 m from the centre of the road during a passage of the truck on the unevenness at a vehicle speed $v = 30$ km/h. Each signal is denoted by a label `FFij`, where `FF`

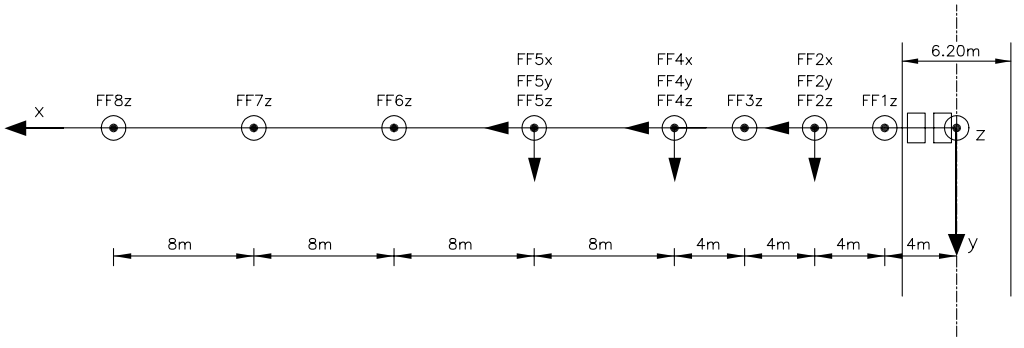

Fig. 14. Position of the measurement line and the accelerometers.

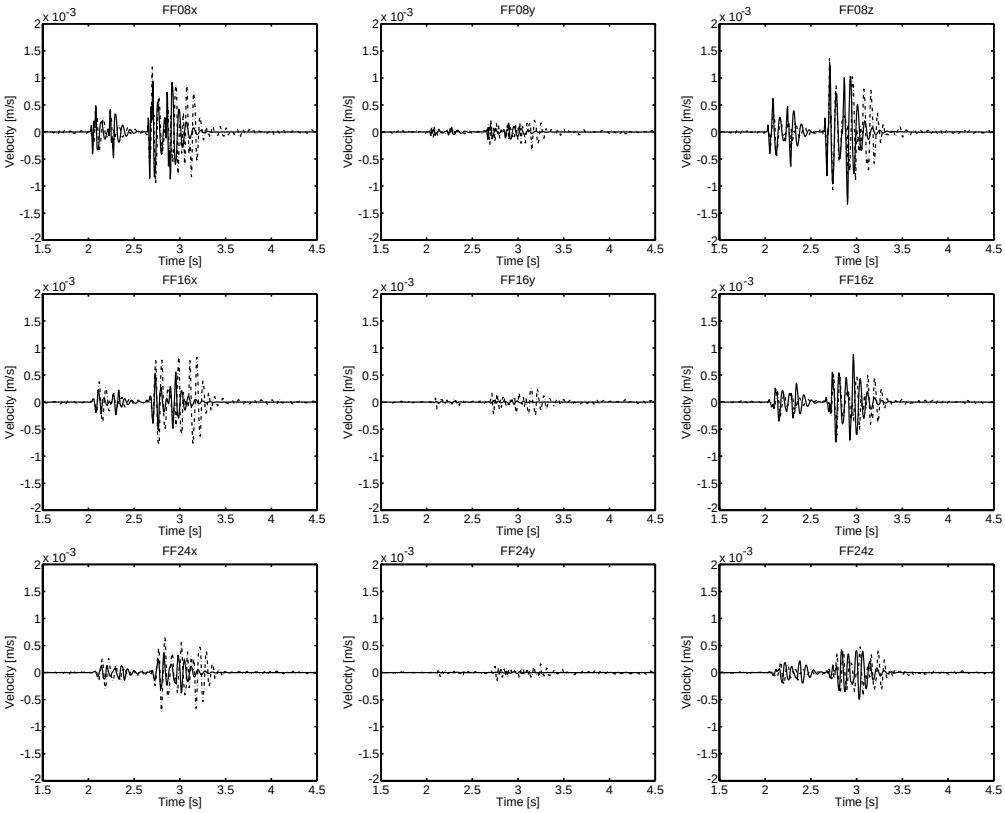

Fig. 15. Time history of the predicted (solid line) and the measured (dash–dotted line) free field velocity at 8, 16 and 24 m for a vehicle speed $v = 30$ km/h.

denotes the free field, i the distance from the source and j the x-, y- or z-component. All signals are shown on the same vertical scale so that the attenuation of the vibrations with distance can better be appreciated.

When the arrival time and the amplitude of the ground vibrations are compared, it can be observed that wave propagation in the soil delays and attenuates the time signals for an increasing distance from the road axis. The time history is composed of the passage of the front and the rear axle on the unevenness, which are well separated in time. As expected, the velocity components v_x and v_z have the same order of magnitude, while v_y is much smaller. The present loading case is similar to the case where a vertical impact is applied at the origin of the reference system. This impact generates waves with an in-plane horizontal component v_x and a vertical component v_z with the same order of magnitude. In the present case, the impacts are not applied at a single fixed position and the in-plane component also contributes to v_y. The latter is also affected by the horizontal component of the interaction force between the vehicle and the road. These observations are confirmed by comments of Taniguchi and Sawada [28] on similar experiments.

The measured and predicted signals correspond well. The main difference is the duration of the transient signal that corresponds to the passage of the rear axle on the profile. This is due to the impact that follows the loss of contact between the rear axle and the road. This phenomenon is

not taken into account with the linear vehicle model. This impact, however, does not generate vibration levels higher than those during the ascending of the rear axle on the profile.

The quality of the prediction varies with the distance x. At 8 m, the measured and predicted velocities v_x and v_z have the same order of magnitude. At 16 and 24 m, the horizontal velocity v_x is underestimated. At all distances, v_y is underestimated, which is due to the fact that the y-component of the interaction force between the vehicle and the road is not accounted for. Although not shown on these figures, the vertical velocity v_z is also underestimated at 32, 40 and 48 m from the centre of the road.

Fig. 16 shows the predicted and measured frequency content of the free field velocity during the passage of the truck on the unevenness at a vehicle speed $v = 30$ km/h. The location of the dominant frequency between 10 and 16 Hz is determined by the dominant frequency of the axle loads and the vertical resonance of the soil at this site. The spectrum is modulated at a wheel base frequency $f_w = v/w = 1.60$ Hz. The frequency content of the predicted and measured signals are mainly situated below 30 Hz and correspond well. Whereas the modulus of v_z is well predicted at all distances, the modulus of v_x and v_y is underestimated at 16 and 24 m. This underestimation is

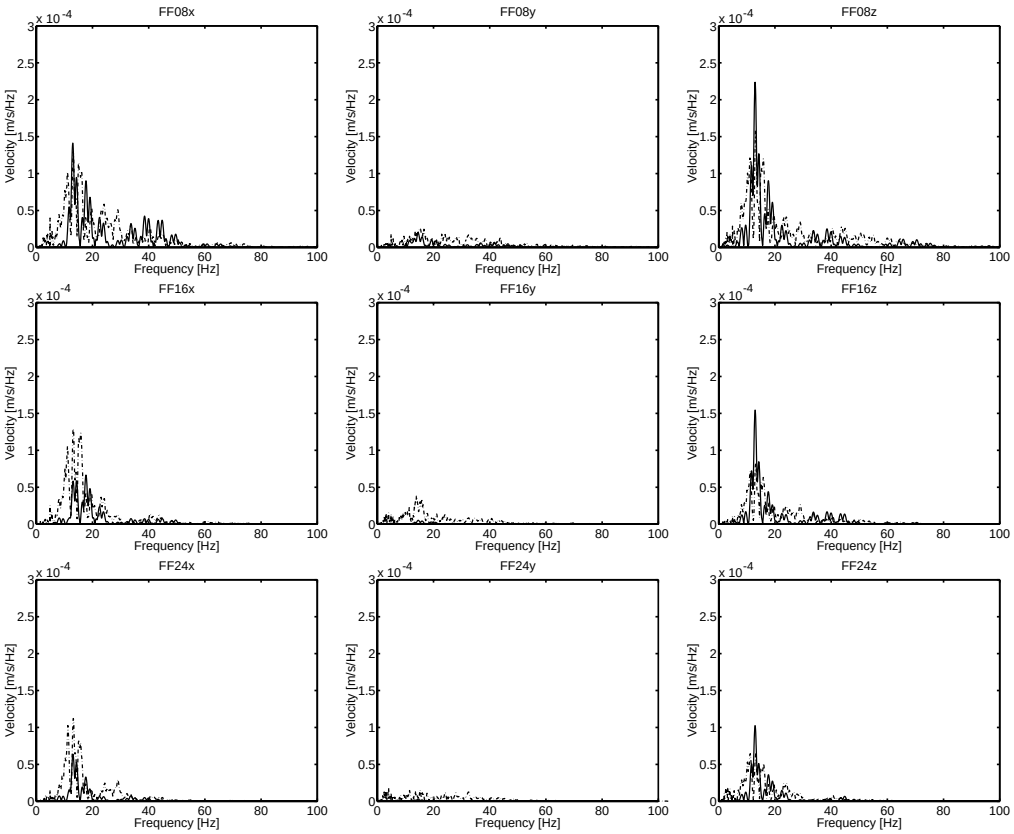

Fig. 16. Frequency content of the predicted (solid line) and the measured (dash–dotted line) free field velocity at 8, 16 and 24 m for a vehicle speed $v = 30$ km/h.

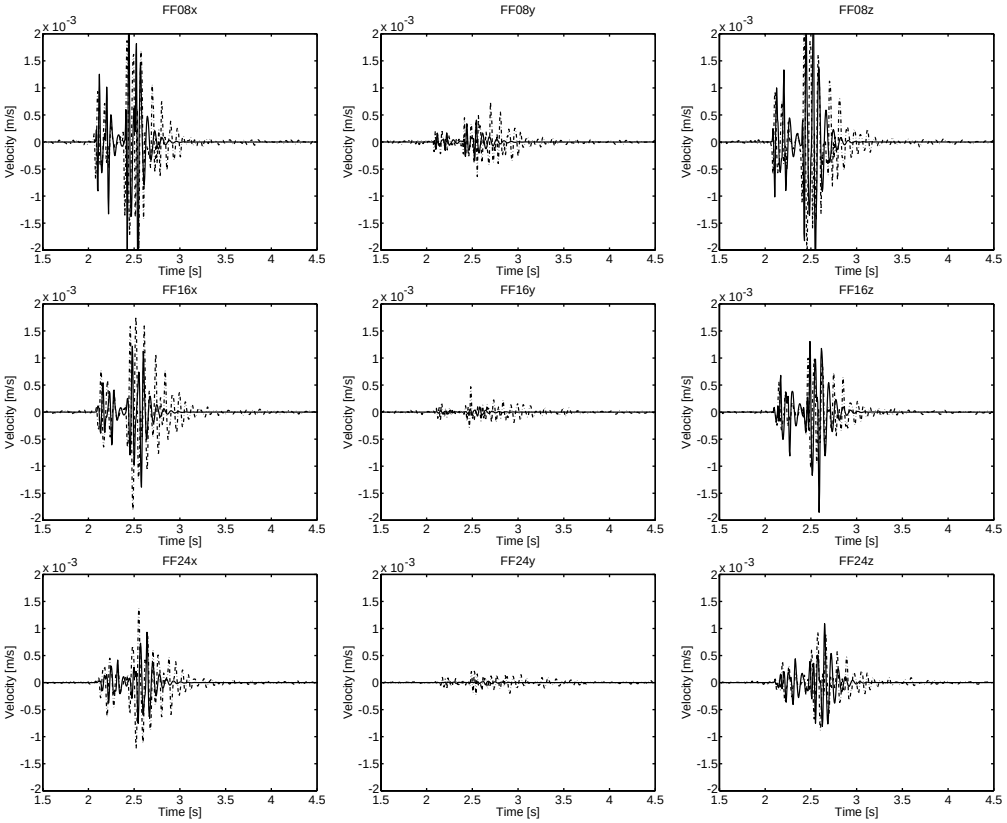

Fig. 17. Time history of the predicted (solid line) and the measured (dash–dotted line) free field velocity at 8, 16 and 24 m for a vehicle speed $v = 58$ km/h.

influenced by both the underestimation of the peak value of the response in the time domain and the larger duration of the measured signal.

Figs. 17 and 18 show similar results for a vehicle speed v equal to 58 km/h. A comparison of the time history shows that the time delay between the impact of the front and the rear axle decreases for higher vehicle speeds, while the PPV is larger at the highest vehicle speed. The quality of the prediction is good for v_x and v_z, while the smaller component v_y is underestimated. Although the loss of contact is not predicted, the measured and predicted PPV have the same order of magnitude.

For an increasing vehicle speed, the frequency content shifts to higher frequencies. The dominant frequency is relatively unaffected and is situated between 10 and 20 Hz. The wheel base frequency $f_w = v/w$ increases linearly with the vehicle speed v and is equal to $f_w = 3.10$ Hz at $v = 58$ km/h. The predicted and measured frequency content correspond well.

5.2. *Peak particle velocity of the free field response*

Fig. 19 shows the predicted and measured peak particle velocity (PPV) as a function of the vehicle speed for all components at a distance x of 8, 16 and 24 m. Fig. 20 shows, additionally, the

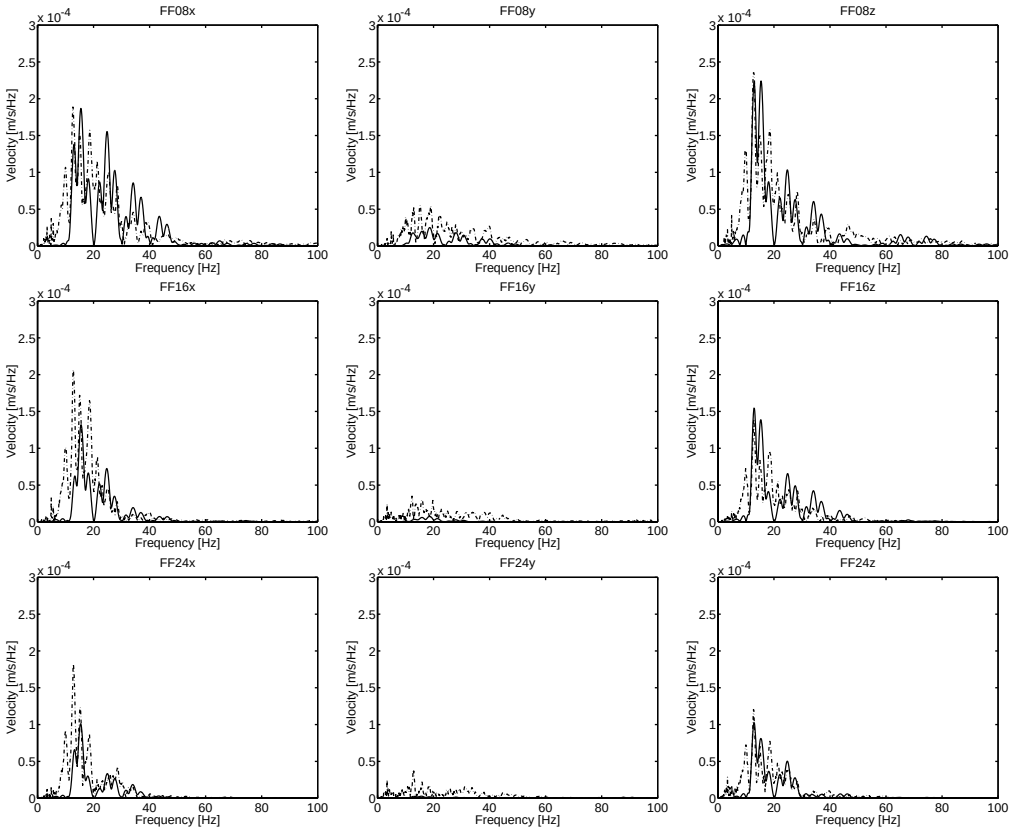

Fig. 18. Frequency content of the predicted (solid line) and the measured (dash–dotted line) free field velocity at 8, 16 and 24 m for a vehicle speed $v = 58$ km/h.

PPV in the vertical direction at 32, 40 and 48 m from the centre of the road. The vertical scale is the same for all figures. These results confirm that the PPV in the x and z direction have the same order of magnitude, while the PPV in the y direction is much smaller. The PPV generally increases with the vehicle speed. The highest vibration levels are generated by the passage of the rear axle on the unevenness. As a result, the PPV of the free field response and the peak acceleration vary in a similar way with the vehicle speed v.

Although the peak acceleration of the rear axle is underestimated at high vehicle speeds, the vertical PPV at 8 and 16 m from the centre of the road is overestimated in the same range of vehicle speeds. The ratio between the predicted and the measured PPV in the x and z direction varies between 0.50 and 1.50 at a distance between 8 and 24 m from the centre of the road. The quality of the prediction of the PPV in the y direction is less good. At larger distances, the PPV is underestimated for all vehicle speeds. The underestimation of the response increases with the distance x from the road. The material damping in the soil is a parameter that affects the response considerably at a large distance from the source. The variation of the quality of the prediction with the distance is therefore probably due to an overestimation of the material damping.

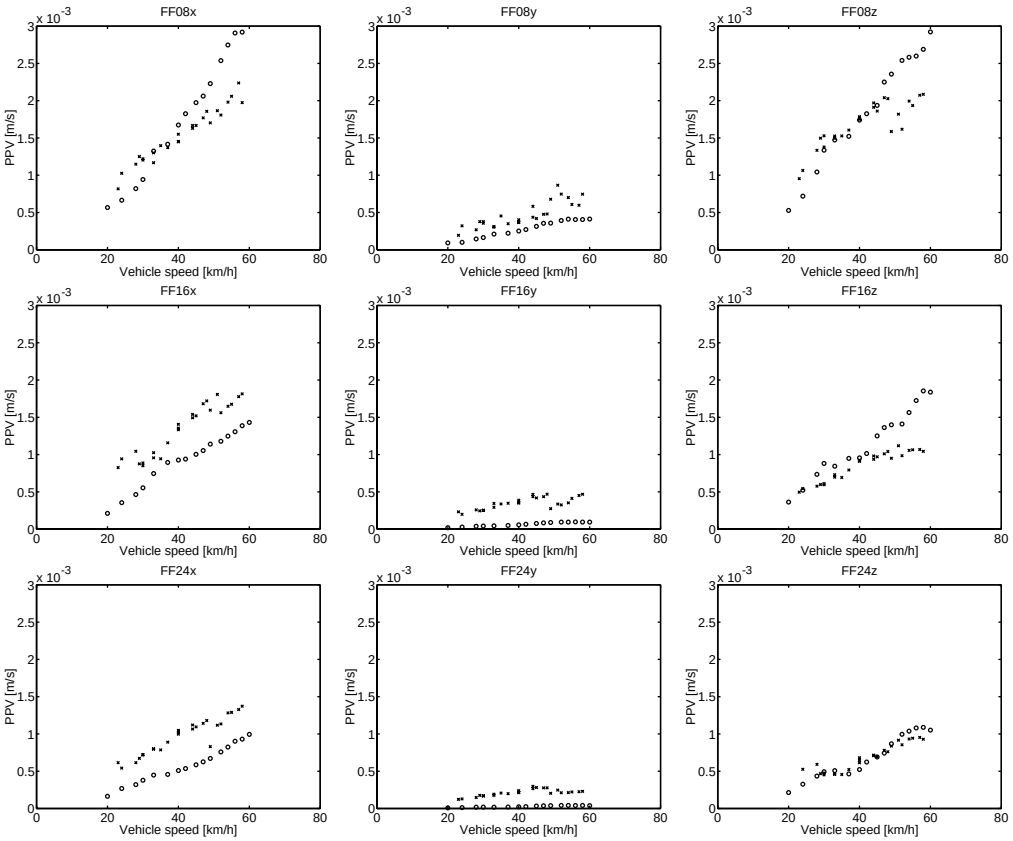

Fig. 19. Predicted (circles) and measured (crosses) peak particle velocity of the free field response at a distance x equal to 8, 16 and 24 m as a function of the vehicle speed.

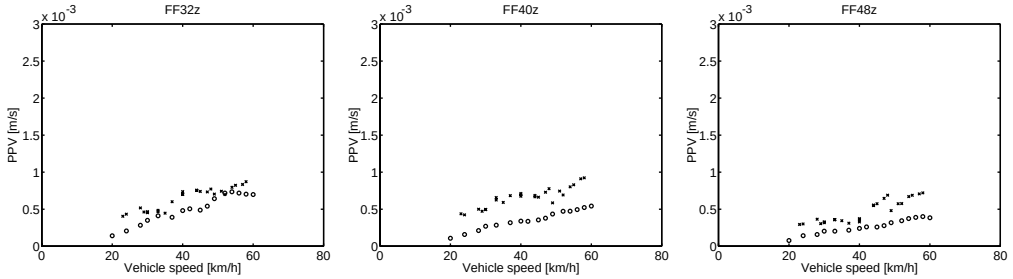

Fig. 20. Predicted (circles) and measured (crosses) peak particle velocity of the vertical free field response at a distance x equal to 32, 40 and 48 m as a function of the vehicle speed.

6. Conclusion

Simultaneous vehicle and free field response measurements allow for a rigorous validation of the prediction model for free field traffic-induced vibrations. The results provide a clear insight in the influence of the vehicle speed on both the vehicle's response and the free field response.

The variation of the vehicle's response and the free field response with the vehicle speed is determined by the shape of the unevenness and the dynamic vehicle characteristics. The peak value of the response generally increases with the vehicle speed, while the frequency content shifts to higher frequencies. The dominant frequencies are relatively unaffected.

A comparison between the predicted and measured response shows that the axle accelerations are well reproduced by the vehicle model. The most important difference is due to the loss of contact between the rear axle and the road.

The time histories of the ground vibrations illustrate that wave propagation in the soil delays and attenuates the free field vibrations. The present load case is similar to the one where a fixed vertical impact load is applied at the origin of the measurement line. The in-plane horizontal component v_x, perpendicular to the road, almost has the same order of magnitude as the vertical component v_z. The out-of-plane horizontal component v_y, parallel to the road, is much smaller. The results therefore demonstrate that the influence of the horizontal interaction force between the vehicle and the road is small. However, as only the vertical component of the interaction force between the vehicle and the road is taken into account for the prediction, the small y-component is underestimated.

The results of the validation are very satisfactory. The velocity components v_x and v_z are well predicted with a ratio of 0.50–1.50 between the predicted and the measured PPV at distances between 8 and 24 m from the centre of the road. The quality of the prediction varies with the distance from the road's axis due to the lack of knowledge about the *in situ* material damping.

The experimental validation shows that the prediction model describes the essential physical phenomena with very reasonable accuracy. The model is therefore well suited to perform a parametric study and to predict free field traffic-induced vibrations. Furthermore, the present numerical model is presently coupled to a receiver model. Such a coupled model allows the response of buildings due to traffic induced vibrations to be predicted and to further investigate the determining factors for traffic-induced vibrations in buildings.

Acknowledgements

The results presented in this paper have been obtained within the 'OROS European University Millennium Award' project 'Vehicle response measurements as a validation tool for a prediction model for free field traffic-induced vibrations'.

The theoretical model has been developed within the research project MD/01/040 'The study of determining factors for traffic induced vibrations in buildings'. The support of the Prime Minister's Services of the Belgian Federal Office for Scientific, Technical and Cultural Affairs is gratefully acknowledged.

References

[1] D. Cebon, Interaction between heavy vehicles and roads, SP-951, L. Ray Buckendale Lecture, SAE, 1993.

[2] T.D. Gillespie, S.M. Karamihas, M.W. Sayers, M.A. Nasim, W. Hansen, N. Ehsan, D. Cebon, Effects of heavy-vehicle characteristics on pavement response and performance, Technical Report 353, NCHRP, Transportation Research Board, Washington, DC, 1993.

[3] W.M.G. Courage, Bronmodel wegverkeer, Technical Report 93-CON-R0056-04, Nederlandse Organisatie voor Toegepast Natuurwetenschappelijk Onderzoek, September 1993.
[4] H. Hao, T.C. Ang, Analytical modelling of traffic induced ground vibrations, Journal of the Engineering Mechanics Division, Proceedings of the American Society of Civil Engineers 124 (8) (1998) 921–928.
[5] H.E.M. Hunt, Stochastic modelling of traffic induced ground vibration, Journal of Sound and Vibration 144 (1) (1991) 53–70.
[6] C.U.R., Prognosemodel trillingshinder, Technical Report 95-2, Civieltechnisch Centrum Uitvoering Research en Regelgeving, 1995.
[7] C.J. Dodds, J.D. Robson, The description of road surface roughness, Journal of Sound and Vibration 31 (2) (1973) 175–183.
[8] ISO8608, Mechanical vibration, road surface profiles, Reporting of measured data, 1991.
[9] M.O. Al-Hunaidi, J.H. Rainer, Remedial measures for traffic induced vibrations at a residential site. Part 1: field tests, Canadian Acoustics/Acoustique Canadiennne 19 (1) (1991) 3–13.
[10] G.R. Watts, Groundborne vibrations generated by HGVs—effects of vehicle, road and ground parameters, Proceedings of the Institute of Acoustics 11 (5) (1989) 99–109.
[11] G.R. Watts, V.V. Krylov, Ground-borne vibrations generated by vehicles crossing road humps and speed control cushions, Applied Acoustics 59 (2000) 221–236.
[12] G. Lombaert, G. Degrande, D. Clouteau, Numerical modelling of free field traffic induced vibrations, Soil Dynamics and Earthquake Engineering 19 (7) (2000) 473–488.
[13] D. Aubry, D. Clouteau, G. Bonnet, Modelling of wave propagation due to fixed or mobile dynamic sources, in: N. Chouw, G. Schmid (Eds.), Workshop Wave '94, Wave Propagation and Reduction of Vibrations, Rühr University, Bochum, Germany, December 1994, pp. 109–121.
[14] G. Lombaert, G. Degrande, Experimental validation of a numerical prediction model for free field traffic induced vibrations by in situ experiments, Soil Dynamics and Earthquake Engineering 21 (6) (2001) 485–497.
[15] G. Lombaert, G. Degrande, Vehicle response measurements as a validation tool for a prediction model for free field traffic induced vibrations, Final report, Report BWM-2001-05, Department of Civil Engineering, Katholieke Universiteit Leuven, March 2001; DWTC Programme Sustainable Mobility, Project MD/01/040, OROS European University Millennium Award.
[16] G. Lombaert, G. Degrande, Study of determining factors for traffic induced vibrations in buildings, Final report, Report BWM-2001-06, Department of Civil Engineering, Katholieke Universiteit Leuven, July 2001; DWTC Programme Sustainable Mobility, Project MD/01/040.
[17] H.E.M. Hunt, Modelling of road vehicles for calculation of traffic induced ground vibrations, Journal of Sound and Vibration 144 (1) (1991) 41–51.
[18] M.O. Al-Hunaidi, J.H. Rainer, Control of traffic induced vibration in buildings using vehicle suspension systems, Soil Dynamics and Earthquake Engineering 15 (1996) 245–254.
[19] M.O. Al-Hunaidi, M. Tremblay, Traffic induced building vibrations in Montréal, Canadian Journal of Civil Engineering 24 (1997) 736–753.
[20] D. Clouteau, MISS Revision 2.1, Notice Utilisateur, Laboratoire de Mécanique des Sols, Structures et Matériaux, Ecole Centrale de Paris, 1993.
[21] G. Degrande, G. De Roeck, P. Van den Broeck, D. Smeulders, Wave propagation in layered dry, saturated and unsaturated poroelastic media, International Journal of Solids and Structures 35 (34–35) (1998) 4753–4778 (Poroelasticity Maurice A. Biot memorial issue).
[22] E. Kausel, J.M. Roësset, Stiffness matrices for layered soils, Bulletin of the Seismological Society of America 71 (6) (1981) 1743–1761.
[23] B. Peeters, G. De Roeck, Reference based stochastic subspace identification in civil engineering, Inverse Problems in Engineering 8 (1) (2000) 47–74.
[24] W. Haegeman, Verslag en interpretatie van de SASW proef en seismische sonderingen op de terreinen van het militair domein te Heverlee, XI.0045, Laboratorium voor Grondmechanica, Universiteit Gent, 2001.
[25] D.K. Watson, R.K.N.D. Rajapakse, Seasonal variation in material properties of a flexible pavement, Canadian Journal of Civil Engineering 27 (1) (2000) 44–54.

[26] O.C.W., Handleiding voor het dimensioneren van wegen met een bitumineuze verharding, volume O.C.W.-A 49/83. 1983.

[27] G. Lombaert, G. Degrande, Determination of the dynamic soil characteristics with the SASW method at the 'de Hemptinne' site in Heverlee, Report BWM-2000-11, Department of Civil Engineering, Katholieke Universiteit Leuven, September 2000, DWTC Programme Sustainable Mobility, Project MD/01/040, OROS European University Millennium Award.

[28] E. Taniguchi, K. Sawada, Attenuation with distance of traffic induced vibrations, Soils and Foundations 19 (2) (1979) 15–28.